Journal of Trace Elements in Medicine and Biology 51 (2019) 65–72

Contents lists available at ScienceDirect

Journal of Trace Elements in Medicine and Biology

journal homepage: www.elsevier.com/locate/jtemb

Analytical methodology

A new ferrous diflunisal complex and its effects on biopools of labile iron

Luca Michael Sihn[a], Fernando Menegatti de Melo[b], Henrique Eisi Toma[b], Silvia Helena Pires Serrano[c], Breno Pannia Espósito[a,*]

[a] Laboratory for Bioinorganic Chemistry and Metallodrugs, Brazil
[b] Supramolecular Nanotech Lab, Brazil
[c] Laboratory of Bioelectrochemistry and Bioelectroanalytical Chemistry, Department of Fundamental Chemistry, Institute of Chemistry, University of São Paulo, Av. Prof. Lineu Prestes 748, São Paulo, SP 05508-000, Brazil

ARTICLE INFO

Keywords:
Iron
Diflunisal
Overload
Chelation

ABSTRACT

Drugs bearing metal-coordinating moieties can alter biological metal distribution. In this work, a complex between iron(II) and diflunisal was prepared in the solid state, exhibiting the following composition: [Fe(diflunisal)$_2$(H$_2$O)$_2$], (Fe(dif)$_2$). The ability of diflunisal to alter labile pools of both plasmatic and cellular iron was investigated in this work. We found out that diflunisal does not increase the levels of redox-active iron in plasma of iron overloaded patients. However, diflunisal efficiently carries iron into HeLa or HepG2 cells, inducing an iron-catalyzed oxidative stress.

1. Introduction

Diflunisal (dif, Dolobid®; Fig. 1) is a nonsteroidal anti-inflammatory drug (NSAID) derived from salicylic acid, displaying a prolonged analgesic effect, requiring usually a single daily dose administration. Despite being used in the management of postoperative dental, orthopedic and gynecological pain [1], diflunisal has been suggested for the treatment of amyloidogenic transthyretin amyloidosis [2] and resistant strains of *Staphylococcus aureus* [3].

Thalassemias are genetic disorders associated to the abnormal production of hemoglobin. Depending upon the mutation, one or more hemoglobin subunits are affected, giving rise to a range of clinical manifestations from the mild thalassemia trait (thalassemia minor, often asymptomatic) to thalassemia major, which requires frequent blood transfusions [4]. Organ damage due to iron overload is an unavoidable side effect of this intervention, as labile iron (highly reactive and potentially redox-active forms of iron) rapidly overwhelms the storage capacity of the body [5]. Iron overload must therefore be treated by iron chelators such as desferrioxamine, deferiprone or deferasirox [6,7]. In addition, chronic pain is a well-documented effect of thalassemia complications. While the precise cause is not generally known, skeletal changes and expansion of the bone marrow, which may be associated to side effects of chelation therapy, as well as low levels of hemoglobin prior to the transfusion may all trigger pain. This can be managed in many patients by the administration of NSAIDs [8].

Being an analog of salicylic acid, diflunisal is a good metal ion chelator, and a number of mononuclear or dinuclear metal-diflunisal complexes has been reported [9,10]. However, to the best of our knowledge, complexes of diflunisal with ferrous iron have not been described yet. This observation has prompted the investigation of the subject, starting from the synthesis and characterization of the complex Fe(dif)$_2$.

The administration of a NSAID which is also a good iron chelator may have a significant impact on the biological redistribution of the metal [7]. For this reason, as a second objective we studied the effect of diflunisal on the properties of reservoirs of labile iron, both plasmatic (LPI, labile plasma iron [11]) and cytosolic (LCI, Labile Cell Iron [6]).

2. Materials and methods

2.1. Materials and instruments

2.1.1. Chemicals

Hepes, NaCl, dimethyl sulfoxide (DMSO), nitrilotriacetic acid (NTA), diethylenetriaminepentaacetic acid (DTPA), calcein, ascorbic acid, ferrous ammonium sulfate (FAS) and $FeSO_4.7H_2O$ were from Sigma-Aldrich. 2′,7′-Dichlorofluorescin diacetate (DCFDA) was available from Invitrogen. Dihydrorhodamine 123, dihydrochloride salt (DHR) was supplied by Biotium. 2′,7′-dichlorodihydrofluorescein diacetate (H_2DCFDA) was obtained from ThermoFisher. Desferrioxamine (DFO) was provided by Cristália (Brazil). Diflunisal (dif) and deferiprone (def) were a gift from Apotex (Canada). Salicylaldehyde

* Corresponding author.
E-mail address: breno@iq.usp.br (B.P. Espósito).

https://doi.org/10.1016/j.jtemb.2018.10.001
Received 14 July 2018; Received in revised form 5 September 2018; Accepted 1 October 2018

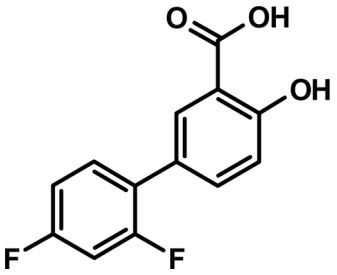

Fig. 1. Structure of diflunisal (dif).

isonicotinoyl hydrazone (SIH) was a gift from Dr. Prem Ponka, McGill University. Hepes Buffered Saline (HBS) was used throughout the work and consisted of Hepes 20 mM, NaCl 150 mM, washed with Chelex®100 (1 g/100 mL) and pH adjusted to 7.4.

2.1.2. Serum samples

Frozen serum samples from patients undergoing hematopoietic stem cell transplantation from a previous study [12] tested for Labile Plasma Iron (LPI) were used. Patients gave their informed consent and the study protocol received approval from the local ethics committee.

2.1.3. Instruments

Elemental analyses (C,H) were performed using a PerkinElmer 2400 series II analyzer. Electronic spectra were recorded on a SpectraMax M4 equipment (Molecular Devices). Fluorescence intensities in microplate experiments were registered with a FluoStar Optima device (BMG). FTIR spectra were registered using a Frontier equipment (PerkinElmer) with samples dispersed in KBr pellets. Thermal analysis coupled with mass spectrometry (TGA-DSC-MS) was performed on a Netzsch thermoanalyser model TGA/DSC 490 PC Luxx coupled to an Aëolos 403 C mass spectrometer using alumina crucibles under synthetic air flow (50 mL/min) and a heating rate of 10 °C/min. All fluorescence measurements were conducted in a FluoStar Optima equipment (BMG) at 485/515 nm (excitation/emission). Magnetic susceptibility was determined by using an experimental Lego® setup as showed previously [13] and a conventional Faraday's method [14]. Electrochemical measurements were obtained using a PGSTAT 101, Potentiotat/Galvanostat from Metrohm AUTOLAB. The data treatment was performed with 1.10.4. version of NOVA and Origin 8.0 softwares.

2.2. Solid state studies

2.2.1. Synthesis of $[Fe(dif)_2(H_2O)_2]$, $\mathbf{Fe(dif)_2}$

The procedure was adapted from the literature for the preparation of a copper(II)-diflunisal derivative [9]. An aliquot of $FeCl_2$ 0.4 M in methanol was allowed to react under stirring with 15 mL of a solution of diflunisal (0.267 M) and KOH (0.16 M). Immediately it was observed the development of a deep blue color. The mixture reacted ~1 h at room temperature and transferred to a refrigerator in order to obtain the crystals of the complex (~ 3 weeks). The crystals were removed and washed with a minimum amount of cold methanol under dry ice. Finally, they were dried under vacuum at room temperature for 3 h.

2.2.2. Computed geometry and molecular vibrations

Molecular modeling calculations were performed using *Orca 4.0.1* software. The ground state geometries and the vibrational spectra were carried out employing density functional theory (DFT) [15,16] with B3LYP hybrid functional [17] with def2-SVP basis set for C, O, S and H atoms and def2-TZVP for the Fe atom, with their pseudopotential for the inner shell electrons. The assignment of the Infrared spectra and supposed structures were carried out using *Gabedit 2.4.0* and *Avogadro 1.2.0* softwares respectively. Unfortunately, in spite of our many attempts, the structure determination has not yet been successful, presumably because of the poor crystal characteristics, sensitive to moisture and dryness, and the presence of labile water molecules which can be randomly oriented.

2.3. Solution studies

2.3.1. Spectrophotometric titration

In flat bottom, transparent 96-well microplates, 168 mL aliquots of aqueous ferrous ammonium sulfate (FAS) 2.4 mM were treated with 32 mL of diflunisal (0–50 mM in DMSO). Final concentrations were 2 mM in iron and 0–8 mM in diflunisal (16% DMSO). After 24 h at room temperature in the dark, the electronic spectra were registered.

2.3.2. Electrochemical studies

Cyclic voltammograms were recorded to evaluate the iron oxidation state of the complex obtained in solution. All voltammograms were obtained in DMSO solutions containing 0.1 M tetrafluoroborate tetrabutylammonium (supporting electrolyte) using glassy carbon, Pt and Ag/AgCl, $KCl_{(sat)}$ as working, auxiliary and reference electrodes, respectively. The glassy carbon electrode was previously polished using diamond spray (from Buhler), 1.0 and 0.3 particle sizes on a TexMet C polishing Pad (also from Buehler). Briefly, 500 µL of 10 mM diflunisal; 10 mM $(Fe(dif)_2$ or 10 mM iron(III) salicylate complex $(Fe(Saly)_3)$ solutions in DMSO were individually added to the electrochemical cell containing 9.5 mL of supporting electrolyte solution, previously deaerated during 15 min by N_2 bubbling.

2.3.3. Effect of diflunisal in Labile Plasma Iron (LPI)

Duplicate plasma samples from either iron overloaded or iron normal patients were treated with ascorbic acid (40 µM) and the probe DHR (50 µM) in HBS, according to a described protocol to assess the amount of LPI in iron overloaded patients [11]. The samples were treated with diflunisal, the standard chelator deferiprone, or a mixture of both. The concentration of each chelator was always 100 µM. After mixture the fluorescence was registered for 1 h at 37 °C in a BMG microplate reader set for fluorescein reading. The slopes of the oxidation rate curves were obtained after fluorescence stabilization (~ 15 min).

2.4. Cell studies

2.4.1. Cell lines and culture

Human cervical carcinoma cell line HeLa was obtained through donation. Human hepatoma cell line HepG2 was purchased from Banco de Células do Rio de Janeiro (BCRJ Catalogue Number 0103). Both were cultivated under 5% CO_2 atmosphere at 37 °C in DMEM (Dulbecco's Modified Eagle's medium containing high glucose), supplemented with 10% fetal bovine serum, 1% L-glutamine and 1% antibiotics (penicillin 10,000 U.I.mg.mL^{-1}, streptomicin 10 mg.mL^{-1} and amphotericin B 1 mg.mL^{-1}). Medium and supplements were purchased from Vitrocell/Embriolife, Brazil. After attaining 80–90% confluence, the cells were tripsinized (Tripsin/EDTA 250 mg.L^{-1}) and seeded (5000 per well) in 96-well microplates coated with 2% clear commercial source gelatin [18] to improve adhesion. The microplates were kept for 48 h in the incubator, prior to the experiments. Then, the medium was removed mechanically from the microplate and the wells were washed twice with 100 µL HBS in order to remove traces of the phenol red indicator.

2.4.2. Cell delivery of iron mediated by diflunisal

Cells received 100 µL of acetomethoxy calcein (CAL-AM; 3 µM in indicator-free growth medium) and were kept for 20 min in the incubator. The wells were washed once with 100 µL HBS and treated with 100 µM of warm probenecid (0.5 mM in HBS) to reduce cell leakage of the fluorescent probe. The microplate was carried into the BMG reader and fluorescence was registered for ~60 min (37 °C; $\lambda_{exc}/\lambda_{em}$ = 485/520 nm). At specified times, 2 µL of stock solutions of the iron

compounds were added, and fluorescence reading was continued until signal stabilization. Demetallation of intracellularly chelated iron was achieved by the addition of 2 μL of SIH 2.5 mM. This experiment was performed in duplicates [19].

2.4.3. Intracellular increase of redox-active iron

Cells received 100 μL of HBS and 6.4 μL of the solution of iron compound to attain the desired final concentration of 7.5 μM. These plates were incubated for 20 min, and during this time it was prepared a fresh H_2O_2 solution 50 μM in HBS supplemented with 10 mM glucose. Plates were washed once with DTPA 100 μM to remove excess iron and treated sequentially with 100 μL of the peroxide solution and 2 μL of DCFDA 1 mM in DMSO. The microplate was carried into the BMG reader and fluorescence was registered (37 °C; l_{exc}/l_{em} = 485/520 nm). After 20 min, 2 μL of SIH 2.5 mM was added to stop the generation of redox-active species catalyzed by iron. The slopes (fluorescence rate/iron concentration) before and after SIH addition were obtained. This experiment was performed in duplicates [20].

3. Results and discussion

3.1. Solid state studies

The complex $Fe(dif)_2$ was obtained in solid state as a deep blue, hygroscopic compound. Elemental analysis indicate the formation of 1:2 (metal:ligand) diaqua compound $[Fe(diflunisal)_2(H_2O)_2]$ or $Fe(dif)_2$ (%C, %H theoretical: 52.91; 3.07. %C, %H experimental: 52.09; 2.83), and further stoichiometric confirmation was attained by means of thermogravimetric analysis.

DTG/DSC analysis under synthetic air, followed by mass spectrometry identification of the volatiles (Fig. 2), shows that water molecules are lost until T_1 = 150 °C. At this temperature, 95% of the initial mass remains, which agrees with the calculated for the loss of two water molecules from $[Fe(diflunisal)_2(H_2O)_2]$ (calculated mass% remaining: 94%). A major decomposition of the organic moiety is observed at ~400 °C as evolution of CO_2. At the higher temperature T_2 = 600 °C only 15% of the initial mass are present, which agrees with $Fe(dif)_2$ being calcined to Fe_2O_3 (calculated mass% remaining: 14%). Despite the synthesis of $Fe(dif)_2$ being conducted in methanol, no signal of this solvent was detectable in our experiment. Finally, the ionization source probably was not strong enough to produce positively-charged fluorine fragments (HF or F_2), which explains their absence from the mass spectra.

The binding mode of diflunisal to Fe(II) was studied by means of infrared (IR) spectroscopy. The experimental IR spectra of diflunisal and $[Fe(dif)_2(H_2O)_2]$ complex are shown in Fig. 3. Diflunisal exhibits a broad and intense band (2500-3500 cm^{-1}) associated with carboxylic and phenol OH groups presumably involved in intramolecular and intermolecular hydrogen bonding. The asymmetric stretching mode of the −COOH group is prominent at 1689 cm^{-1}, while the corresponding symmetric mode can be located at 1588 cm^{-1}. The remaining bands are associated with the vibrational modes of the aromatic rings and C–F groups and are not particularly relevant for the discussion of the complex structure. In the case of the $Fe(dif)_2$ complex, an additional strong peak is observed in the (2500-3500 cm^{-1}) region, corresponding to the O—H stretching modes of coordinated water molecules. The H—O—H bending modes are located at 1615 cm^{-1}. In contrast with the diflunisal spectrum, the ν(COOH) peak at 1689 cm^{-1} disappears, and a careful comparison with the two spectra allows to locate the $\nu_{as}(-COO)$ and $\nu_s(-COO)$ peaks at 1594 and 1504 cm^{-1}. The frequency separation (Δν) of these two vibrational peaks has been used to assign the binding modes of the carboxylate group in coordination compounds. Generally, there are three basic modes of coordination of the carboxylate group to the metal ions: a) monodentate binding, b) bridging and c) bidentate binding. In the monodentate coordination mode, Δν is usually large (200 – 320 cm^{-1}), and for the bridging mode Δν is typically around 150 cm^{-1}. In the case of the bidentate binding, Δν is usually small, around 110 cm^{-1}, as observed for the $Fe(dif)_2$ complex (Δν = 90 cm^{-1}). Most of the vibrational peaks of the aromatic groups are preserved in the FTIR spectra of diflunisal and the iron complex. Additional band observed for the complex are related to the changes in the bending and torsion modes of the coordinated carboxylate groups at 716 and 662 cm^{-1} as well as to the metal-ligand, $M-OH_2$ vibrations at 432 cm^{-1}.

This peculiar carboxylate bidentate binding mode of diflunisal in the complex seems to promote a greater stabilization of the $Fe(dif)_2$ geometry in a nearly planar *trans* configuration, as evidenced by the DFT theoretical simulations carried out in this work (Figures SI-1 and SI-2, see Supplementary Information). The alternative chelating mode, involving the binding of the carboxylic and phenol groups to the iron (II) ion leads to a greater distortion, associated with the formation of a six membered ring, also reflecting the relatively large radius of the metal ion. This situation is expected to change in the case of the iron (III) complex, which is known to form very stable complexes with the salicylate group, because of its smaller size, and strong acidic characteristics.

To confirm the presence of Fe(II) in the complex, we performed some basic magnetic susceptibility measurements. In brief, when an object is placed in a magnetic field, the induced a magnetic moment can be parallel to the external field, if the material is paramagnetic. If the moment is antiparallel to the external field, the material is diamagnetic. In that way, if the magnetization is induced by an external magnetic field, the determination of the volume magnetic susceptibility, allows to estimate the number of unpaired electrons.

The measured magnetic susceptibility for $[Fe(dif)_2(H_2O)_2]$ is 1.9036×10^{-5} cgs. g^{-1} at 23.4 °C, using $[Ni(en)_3]S_2O_3$ as a standard sample. It means that its molar magnetic susceptibility is 1.12362×10^{-2} cgs. mol^{-1}. In that way, the paramagnetic susceptibility of the iron in the complex, considering all diamagnetic contributions of twenty four aromatic carbons, two water molecules, two aliphatic carbons, four fluorine atoms, two hydrogen atoms, four oxygen from hydroxyl groups and two other oxygens coordinating Fe(II) is 1.13274×10^{-2} cgs. By using the spin-only approximation, which is valid for the 3d elements, the effective magnetic moment is 5.20 and, corresponding to four unpaired electrons as expected for Fe(II), d^6, in a high spin configuration.

3.2. Solution studies

For biological systems, ferrous iron is the most bioavailable form, and as such it is absorbed from the intestinal lumen, exported to the bloodstream *via* ferroportin or internalized into the stock protein ferritin for conversion into more stable ferric forms [21,22]. On the other hand, diflunisal is a very insoluble molecule with long plasma half-life and non-linear pharmacokinetics, making it required to be loaded usually in relatively high doses in order to quickly attain steady-state levels [23]. Depending upon the initial prescribed doses, plasma peak levels can be as high as 350–760 μM after an 11-day treatment. Since levels of labile plasma iron (LPI) in iron-overloaded patients can be as high as 20 μM [11], it stands to reason that the interactions between metal and drug may occur *in vivo*.

In this section and in the cell testes, we simulated the formation of iron-diflunisal compounds in biological fluids by promoting the reaction, in buffered medium, of FAS and diflunisal in different stoichiometric proportions (1:1 or 1:2, metal:ligand). FAS was selected since it is more readily soluble and cause less interference with pH than $FeCl_3$ or other simple ferric salts.

A spectrophotometric titration of Fe(II) with diflunisal in DMSO solution is presented in Fig. 4. The λ_{max} of 500 nm, for the 1:1 metal:ligand ratio, was used to monitor the progress of the titration. The maximum metal:ligand ratio attained was 1:2 which agrees with the solid state findings above. Even in the presence of a significant amount of DMSO as a co-solvent, the complex $Fe(dif)_2$ presented itself as a deep blue aqueous solution.

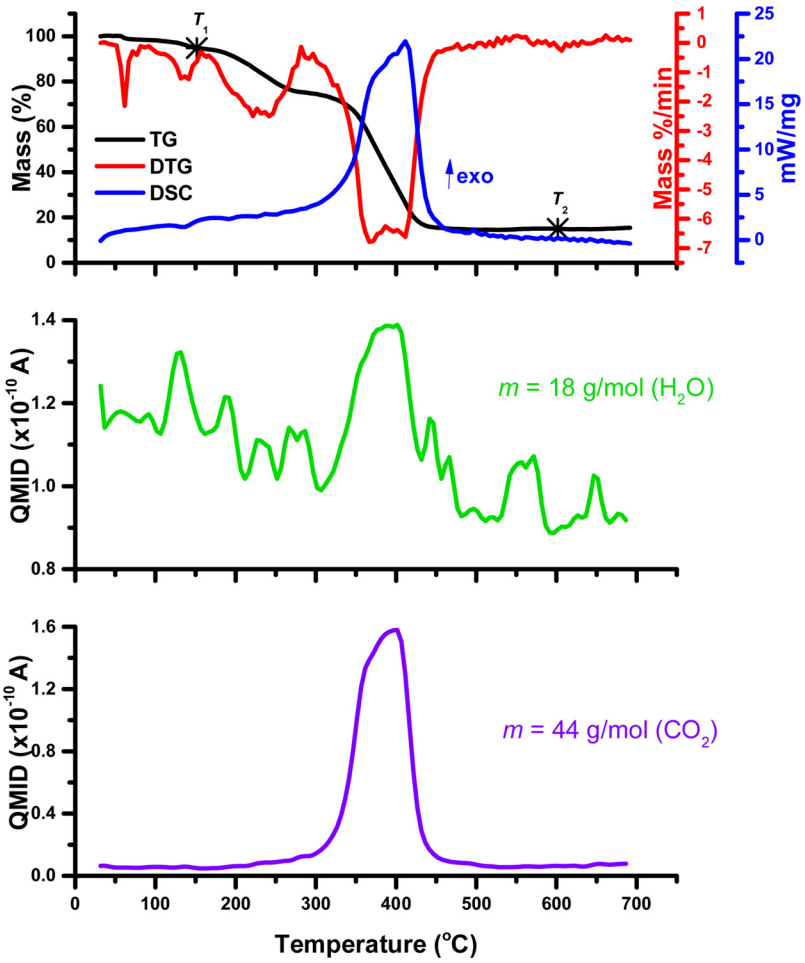

Fig. 2. Upper panel: Thermogravimetric profile and Differential Scanning Calorimetry of $Fe(dif)_2$ under synthetic air. Middle and bottom panels: mass spectra for H_2O and CO_2 emissions, respectively, as a function of temperature.

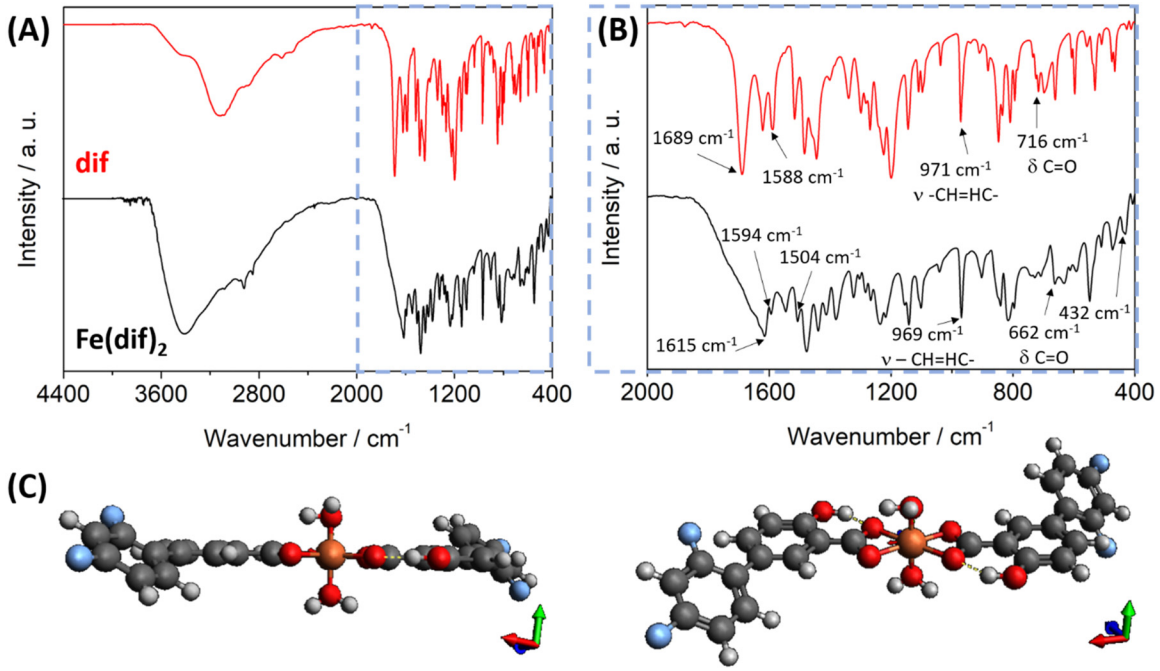

Fig. 3. (A) Experimental diflunisal and $[Fe(dif)_2(H_2O)_2]$ IR spectra. (B) Zoom in from 2000 cm^{-1} to 400 cm^{-1} highlighting 1), 2), 3) and 4) big similar regions from both spectra. (C) Proposed structure for $Fe(dif)_2$ using Avogadro 1.2.0.

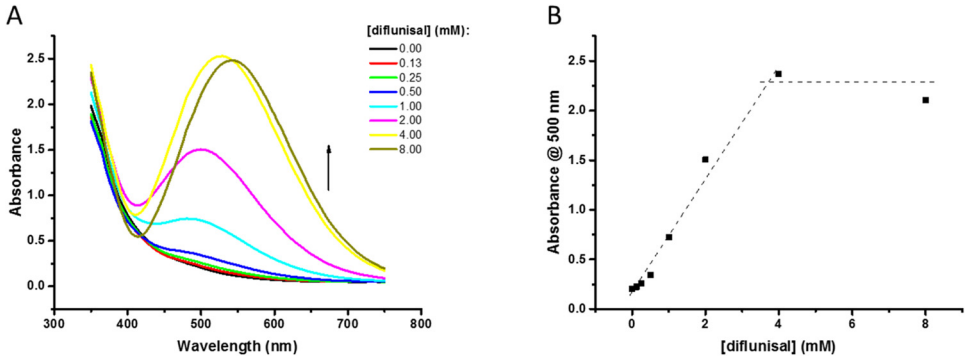

Fig. 4. (A) Electronic spectra for the system Fe(II)–diflunisal. (B) Titration curve. Iron concentration = 2 mM.

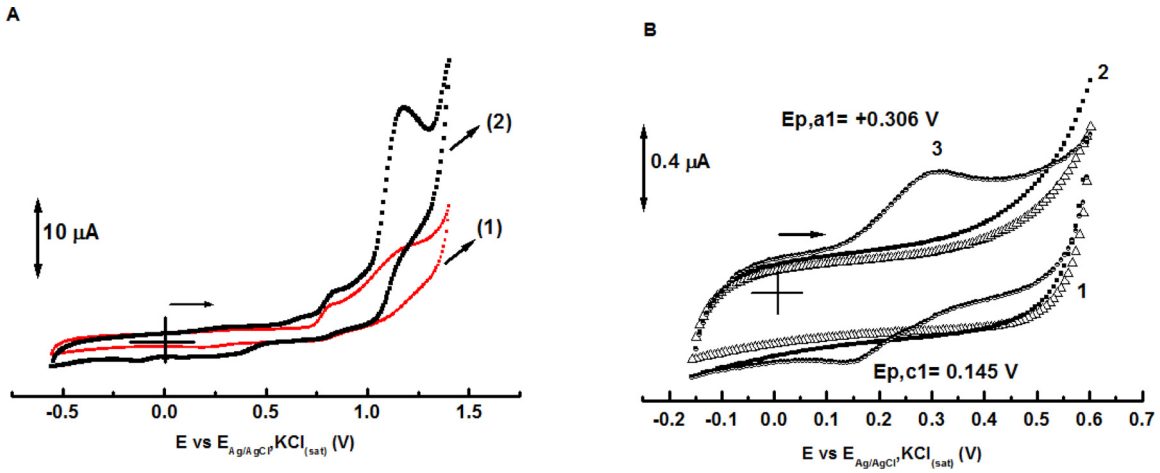

Fig. 5. Cyclic voltammograms of 0.5 mM of diflunisal (A, curve 2) or 0.5 mM of $Fe(dif)_2$ complex (B, curve 3); 0.5 mM $Fe(salyc)_3$ (B, curve 2). (1) is the supporting electrolyte solution (DMSO containing 0.1 mol L^{-1} of tetrabutylammonium tetrafluoroborate). Experimental conditions: **(A)** E_i = 0 V; $*E_{\lambda 1}$ = 1.4 V; $E_{\lambda 2}$ = -0.55 V and E_{final} = 0.0 V. **(B)** E_i = -0.1 V; $E_{\lambda 1}$ = +0.6 V; $E_{\lambda 2}$ = -0.15 V and E_{final} = -0.1 V. at ν = 100 mVs^{-1}. $*E_{\lambda}$ = sweep inversion potential.

Cyclic voltammetry was used to evaluate the iron oxidation state in the complex obtained in solution. Initially, cyclic voltammograms were performed in the diflunisal solution to assess the potential window to be used in the $Fe(dif)_2$ solution to guarantee the integrity of the iron oxidation state in the complex during the electrochemical measurements. Fig. 5 shows the results obtained in 0.5 mM of the ligand and complex solutions.

As can be seen from Fig. 5A, diflunisal presents a main oxidation peak, Ep,a, at +1.18 V and no peak at 0.0 V, and therefore this potential was used as an initial potential to perform the voltammogram of both $Fe(dif)_2$ and ferric salycilate complexe solutions (Fig. 5B).

Fig. 5B shows that $Fe(dif)_2$ presents a very well defined oxidation peak (Epa,1) at +0.306 V, attributed to the oxidation of Fe(II) to Fe(III) in the complex, and a very well defined reduction peak Epc,1 (+0.145 V) in the reverse sweep. The ΔEp (Ep,a – Ep,c) value of +0.161 V characterizes the process as a quasi-reversible [24]. On the other side, the ferric salycilate complex, $Fe(saly)_3$ does not present electrochemical activity on the same applied potential range. In conclusion, the electrochemical results corroborate the spectroscopic data, which indicated that the complex is formed with Fe(II).

The chemical speciation of iron in the bloodstream of iron-overloaded patients is not completely known, involving probably (hydr)oxo derivatives and/or albumin, citrate or hormone complexes [6,25] of mainly iron(III). This collective of iron species is termed *Non-Transferrin Bound Iron* (NTBI), and it may reach levels higher than 10 µM in the plasma of transfused beta-thalassemic patients [6]. However, usually only a fraction of the NTBI is able to engage into redox-active processes leading to oxidative damage, prompted by the reduction of the iron(III) species by endogenous ascorbate and subsequent oxidation of iron(II) by molecular oxygen with concomitant production of reactive oxygen species [11]. This redox-active fraction of NTBI is known as *Labile Plasma Iron* (LPI) [6,11] and is therefore considered an important target of iron-overload chelation therapy. Approved, high affinity chelators (DFO, deferasirox or deferiprone) are all able to bind and keep iron in redox-inactive forms thus reducing the levels of LPI. However, low affinity chelators (such as diflunisal) might inadvertently increase the native levels of LPI by solubilizing and mobilizing NTBI species that were hitherto inert. This has been observed for the relatively mild chelator nitrilotriacetate [26].

In a preliminary study (Fig. 6), it was confirmed that the gold standard deferiprone successfully decreased the levels of LPI in the plasma of iron-overloaded patients, without mobilizing iron from iron-normal patients. This agreed with our previous findings [12]. Diflunisal alone has minor effects on the decrease of LPI (samples # 4 and 6), which do not seem to be additive to the effect of deferiprone. In no instance we observed *increased* LPI levels after the exclusive administration of diflunisal, which would suggest it is not a good mobilizing agent for NTBI.

3.3. Cell studies

The access of LPI/NTBI to cells is a subject of great medical interest, since these iron species elude normal cell controls (e.g., transferrin receptor-mediated absorption) and quickly overcome the ability of cell proteins to stock the surplus metal under safe forms. Several mechanisms by which LPI/NTBI can access cells have been suggested, including hijacking divalent metal transporters (which opens the possibility of using ion channel blockers as an innovative therapy for iron overload

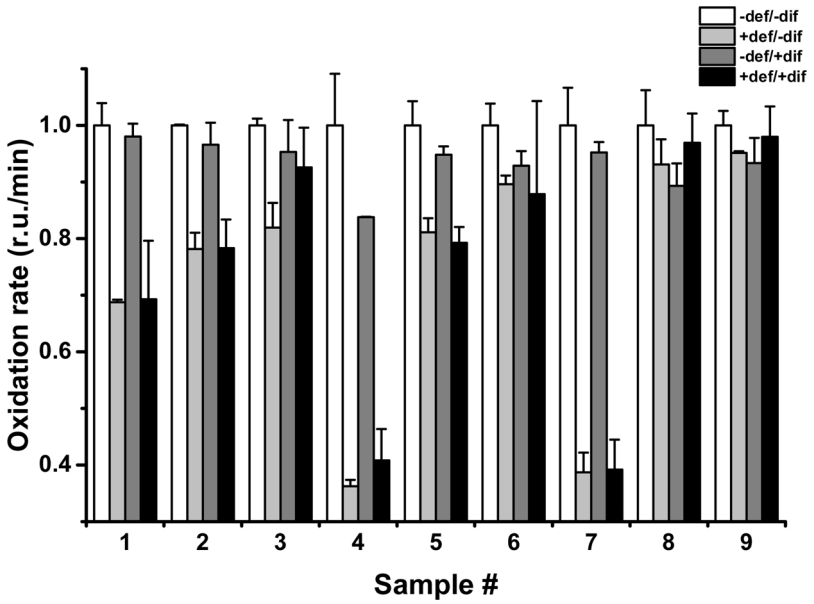

Fig. 6. Oxidation rates of DHR catalyzed by iron in the plasma of both iron-overloaded (# 1–7) and iron-normal (# 8–9) samples, under the effect of combinations of deferiprone (def) or diflunisal (dif) at 100 μM. r.u.: relative units of fluorescence.

[22,27]) or simply following passive diffusion. This could be an important route for highly hydrophobic species such as the iron-diflunisal derivatives under study.

Two cell lineages were chosen to study the permeation of iron, HeLa (as a general model for rapid metabolism) and HepG2 (as a *bona fide* model for liver function, which is one of the first important targets of iron overload [6]). Iron was administered as "free" (as in FAS), chelated with different stoichiometric proportions of diflunisal, or as ferric hydroxyquinoline (FeHQ), which is a standard for rapid, intense iron overload [19]. None of these compounds caused loss of cell integrity after the ~60 min duration of the experiment, assessed by visual inspection of the microplates after the end of each run.

The profiles for cell iron absorption are depicted in Fig. 7 as disturbances in the fluorescence signals. Since calcein concentration is directly proportional to calcein fluorescence, and this in turn is proportional to iron concentration, a calibration curve (Figure SI-3) was used to convert the drop of fluorescence into intracellular iron concentrations (Table 1). These values agree with previous findings for murine hepatocytes, where basal levels of 0.25 mM intracellular iron were almost doubled after exposure to exogenous iron [28].

Table 1
Intracellular iron concentrations (μM) after loading into HeLa or HepG2 cells.

Compound	in HepG2	in HeLa
FAS	0.05	0.42
Fe(dif)	0.11	0.36
$Fe(dif)_2$	0.12	0.30
FeHQ	> 0.36	> 0.55

Different cell types have different metabolic rates and requirements for iron, along with possibly different membrane permeability. In general, HeLa cells were more iron-avid, which is expected considering its high metabolic rate. Diflunisal was able to carry iron to both cell types without meaningful differences between the complexation

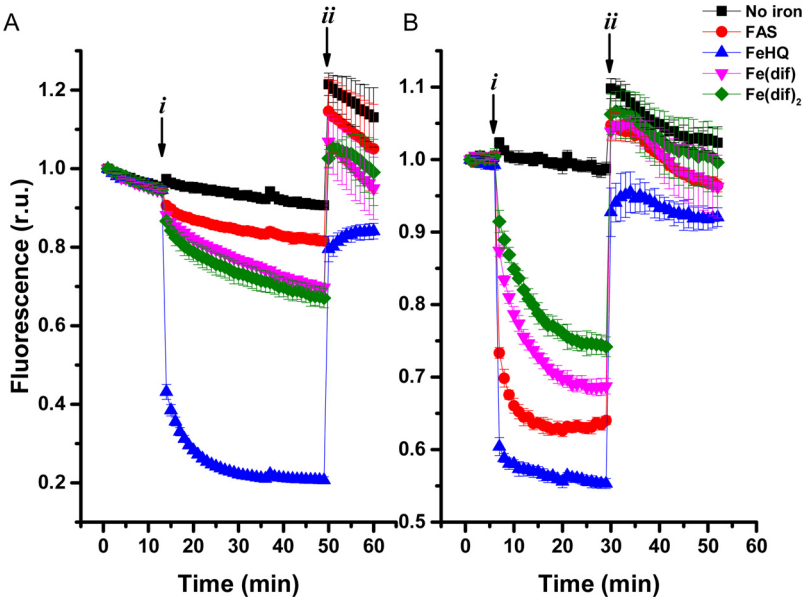

Fig. 7. Fluorescence profiles of calcein loaded into (A) HepG2 or (B) HeLa cells. At time point *i*, iron compounds were added at 20 μM (125 μM for FeHQ) iron concentration. At time point *ii*, the high affinity, cell permeant chelator SIH (50 μM; final concentration) was added to recover the fluorescence as a means to verify the integrity of the fluorescent probe. r.u.: relative units of fluorescence.

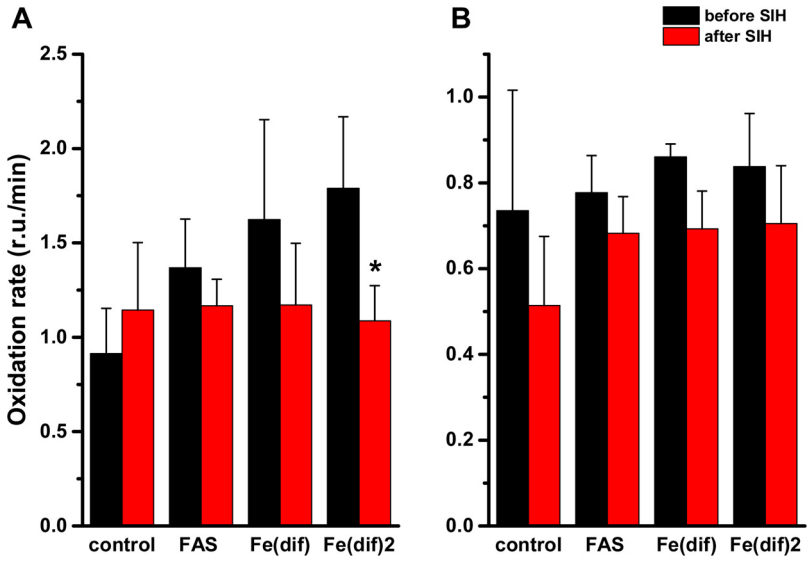

Fig. 8. Oxidation rates of DCFDA in (A) HeLa or (B) HepG2 cells loaded with peroxide and different iron species (7.5 μM), before and after the radical-generating reactions are stopped by the addition of SIH (50 μM; final concentration). r.u.: relative units of fluorescence.

stoichiometry. Curiously, in HepG2 all the iron complexes were more absorbed than FAS, which has probably a controlled absorption. This suggests that plasmatic iron-diflunisal species could be a real iron source for the liver in iron overloaded patients.

Intracellular peroxide may be a trigger for oxidative stress catalyzed by the presence of iron. Indeed, the increase of labile pools of intracellular iron has long been accepted as a major source of tissue damage in iron overloaded patients [29]. The extent of oxidative stress can be inferred by the oxidation rate of fluorescent probes such as DCFDA (Fig. 8). The rationale is that the compounds that mostly carry iron ions to the cell might induce the greater extent of oxidative damage to the probe, and this effect is halted by the administration of exogenous high affinity hexadentate chelator SIH [20]. In HeLa (Fig. 8A) treated with $Fe(dif)_2$ there was a significant decrease of iron-catalyzed oxidative stress after the addition of SIH. In HepG2 (Fig. 8B), despite a similar trend is observed, the results did not attain statistical significance. Combined with the permeability results, this would suggest that diflunisal may ferry redox-active iron to cells. Even though diflunisal, as several other anti-inflammatory drugs, is able to scavenge hydroxyl radicals in solution [30], this effect may be of little beneficial use if the drug itself causes metal overload into tissues.

In conclusion, at therapeutic doses, diflunisal may form iron complexes that are cell-permeant and redox-active.

Declaration of interest

none

Acknowledgments

The authors are indebted to Mrs. Jéssica Esposito for the technical support with the *in vitro* experiments. Dr. Ricardo de Couto obtained the thermogravimetric data. LMS received a grant from National Council for Scientific and Technological Development (CNPq). São Paulo Research Foundation (FAPESP; grants 2016/03709-9 and 2013/24725-4) funded this research.

Appendix A. Supplementary data

Supplementary material related to this article can be found, in the online version, at doi:https://doi.org/10.1016/j.jtemb.2018.10.001.

References

[1] J.O. Wasey, et al., Single dose oral diflunisal for acute postoperative pain in adults, Cochrane Database Syst. Rev. 4 (2010).
[2] H. Jono, Y. Ando, Towards targets and treatments in transthyretin amyloidosis, Expert Opin. Orphan Drugs 5 (9) (2017) 691–699.
[3] V. Khodaverdian, et al., Discovery of antivirulence agents against methicillin-resistant Staphylococcus aureus, Antimicrob. Agents Chemother. 57 (8) (2013) 3645–3652.
[4] J.B. Porter, et al., Limitations of serum ferritin to predict liver iron concentration responses to deferasirox therapy in patients with transfusion-dependent thalassaemia, Eur. J. Haematol. 98 (3) (2017) 280–288.
[5] O. Kakhlon, Z.I. Cabantchik, The labile iron pool: characterization, measurement, and participation in cellular processes, Free Radic. Biol. Med. 33 (8) (2002) 1037–1046.
[6] I.Z. Cabantchik, et al., The Molecular and Cellular Basis of Iron Toxicity in Iron Overload (IO) Disorders. Diagnostic and Therapeutic Approaches, Thalassemia Reports 3 (s1) (2013) e3.
[7] J.B. Porter, Practical management of iron overload, Br. J. Haematol. 115 (2) (2001) 239–252.
[8] A. Lal, Assessment and Treatment of Pain in Thalassemia, editor, Cooley's Anemia, S. New York Acad, 2016, pp. 65–72.
[9] S. Fountoulaki, et al., Non-steroidal anti-inflammatory drug diflunisal interacting with Cu(II). Structure and biological features, J. Inorg. Biochem. 105 (12) (2011) 1645–1655.
[10] S. Tsiliou, et al., Cobalt(II) complexes with non-steroidal anti-inflammatory drugs and alpha-diimines, J. Inorg. Biochem. 160 (2016) 125–139.
[11] B.P. Esposito, et al., Labile plasma iron in iron overload: redox activity and susceptibility to chelation, Blood 102 (7) (2003) 2670–2677.
[12] F.A. Naoum, et al., Assessment of labile plasma Iron in patients who undergo hematopoietic stem cell transplantation, Acta Haematol. 131 (4) (2014) 222–226.
[13] F.M. Melo, et al., Magnetophoresis of superparamagnetic nanoparticles applied to the extraction of lanthanide ions in the presence of magnetic field, NanoWorld J. 3 (2017) 38–43.
[14] B.L. Morris, A. Wold, Faraday Balance For Measuring Magnetic Susceptibility, Rev. Sci. Instrum. 39 (12) (1968) 1937.
[15] P. Hohenberg, W. Kohn, Inhomogeneous Electron gas, Phys. Rev. 136 (3B) (1964) B864–B871.
[16] W. Kohn, L.J. Sham, Self-consistent equations including exchange and correlation effects, Phys. Rev. 140 (4A) (1965) A1133–A1138.
[17] A.D. Becke, Density-functional thermochemistry. V. Systematic optimization of exchange-correlation functionals, J. Chem. Phys. 107 (20) (1997) 8554–8560.
[18] Sigma-Aldrich, Gelatin Cell Attachment Protocol, [cited May 02, 2018]; Available from: (2008) https://www.sigmaaldrich.com/technical-documents/articles/biofiles/gelatin-solution-product.html.
[19] M. Shvartsman, E. Fibach, Z.I. Cabantchik, Transferrin-iron routing to the cytosol and mitochondria as studied by live and real-time fluorescence, Biochem. J. 429 (2010) 185–193.
[20] Y.S. Sohn, et al., Rescuing iron-overloaded macrophages by conservative relocation of the accumulated metal, Br. J. Pharmacol. 164 (2B) (2011) 406–418.
[21] R. Gozzelino, P. Arosio, Iron Homeostasis in Health and Disease, Int. J. Mol. Sci. 17 (1) (2016).
[22] D.S. Kalinowski, et al., Redox cycling metals: pedaling their roles in metabolism and their use in the development of novel therapeutics, Biochim Et Biophys Acta-Mol.

Cell Res. 1863 (4) (2016) 727–748.
[23] AAPharma, Diflunisal, [cited 29/04/18]; Available from: (2014) https://www.aapharma.ca/downloads/en/PIL/2016/Diflunisal-PM.pdf.
[24] C.M.A. Brett, A.M.O. Brett, Electrochemistry: Principles, Methods, and Applications, Oxford Science Publications, 1993.
[25] R.W. Evans, et al., Nature of non-transferrin-bound iron: studies on iron citrate complexes and thalassemic sera, J. Biol. Inorg. Chem. 13 (1) (2008) 57–74.
[26] W. Breuer, et al., Non-transferrin bound iron in Thalassemia: differential detection of redox active forms in children and older patients, Am. J. Hematol. 87 (1) (2012) 55–61.
[27] Y. Zhang, et al., Calcium channel blockers ameliorate iron overload-associated hepatic fibrosis by altering iron transport and stellate cell apoptosis, Toxicol. Appl. Pharmacol. 301 (2016) 50–60.
[28] G. Zanninelli, et al., The labile iron pool of hepatocytes in chronic and acute iron overload and chelator-induced iron deprivation, J. Hepatol. 36 (1) (2002) 39–46.
[29] C.P. Ozment, J.L. Turi, Iron overload following red blood cell transfusion and its impact on disease severity, Biochim Et Biophys Acta-Gen Subj 1790 (7) (2009) 694–701.
[30] O.I. Aruoma, B. Halliwell, The iron-binding and hydroxyl radical scavenging action of anti-inflammatory drugs, Xenobiotica 18 (4) (1988) 459–470.